Structural phase diagram of the $Ba_{1-x}K_xBiO_3$ system

Shiyou Pei, J. D. Jorgensen, B. Dabrowski, D. G. Hinks, D. R. Richards, and A. W. Mitchell
Materials Science Division, Argonne National Laboratory, Argonne, Illinois 60439

J. M. Newsam, S. K. Sinha, D. Vaknin, and A. J. Jacobson
Exxon Research and Engineering Company, Route 22 East, Annandale, New Jersey 08801
(Received 22 August 1989)

The structures of five phases in the $Ba_{1-x}K_xBiO_3$ system for $0 \le x \le 0.5$ and temperatures below 473 K have been determined by neutron powder diffraction. Bulk superconductivity occurs only in a cubic perovskite phase which exists for $x \ge 0.37$ (at 10 K). At room temperature, as the potassium concentration is decreased, the cubic structure distorts first by BiO_6 octahedral tilting and then by symmetric oxygen breathing-mode distortions. Semiconducting behavior for the monoclinic phase at $0 \le x \le 0.1$ can readily be explained on the basis of a commensurate charge-density wave. The semiconducting orthorhombic phase, which extends from the monoclinic phase to the cubic superconducting phase, contains only octahedral tilting distortions that would not be expected to destroy metallic behavior. Thus, this commensurate structure provides no explanation for the metal-insulator transition. An incommensurate modulation extending across the semiconducting region of the phase diagram has been observed by electron diffraction, but is not observed by neutron diffraction. It is not clear whether this incommensurate modulation is responsible for the nonmetallic behavior.

I. INTRODUCTION

Cubic $Ba_{1-x}K_xBiO_3$ exhibits the highest superconducting transition temperature ($T_c = 30$ K for $x \approx 0.4$) reported for any oxide superconductor not containing copper.[1-3] The most striking feature of this compound is the absence of two-dimensional, metal-oxygen planes, which are widely believed to be an essential factor in producing a high T_c in the copper-oxide systems. In addition, local magnetic moments do not exist in these materials. They are diamagnetic[4] and muon spin-resonance data reveal no evidence of static magnetic order.[5] Therefore, magnetic-pairing mechanisms, as proposed for the cuprate superconductors, can be excluded for this material.

Several measurements point to the involvement of phonons in the mechanism for superconductivity in the $Ba_{1-x}K_xBiO_3$ system. The large oxygen-isotope effect, measured by substituting ^{18}O for ^{16}O, is consistent with a phonon-mediated mechanism.[6,7] The superconducting energy gap, measured by infrared reflectivity,[8] is consistent with weak to moderately strong coupling in a Bardeen-Cooper-Schrieffer (BCS) theory. A recent inelastic neutron-scattering measurement and molecular-dynamics simulation of the phonon density of states show that high-energy optical phonons (up to 80 meV) involving only the oxygen atoms are present in this system.[9] The large lattice softening observed at high energies on substituting potassium for barium in insulating $BaBiO_3$ is probably due to strong electron-phonon coupling.[9] The direct coupling of these high-energy optical phonons to the superconducting electronic system has been demonstrated by a recent tunneling measurement.[10] These results are in agreement with BCS phonon-mediated superconductivity in $Ba_{1-x}K_xBiO_3$ with an overall electron-phonon coupling constant (λ) of about unity but with strong coupling to high-energy oxygen optical phonons.[11]

In addition to the lack of two-dimensional structural features and antiferromagnetism, $Ba_{1-x}K_xBiO_3$ exhibits a number of other interesting properties that suggest that important physics can be learned from this system. In common with the cuprate superconductors, superconductivity in $Ba_{1-x}K_xBiO_3$ appears at the boundary of a metal-insulator transition.[3,12,13] Superconductivity occurs only in a cubic phase ($x \ge 0.37$) and disappears abruptly upon crossing a phase transition to a semiconducting phase when the potassium concentration is decreased.[3,12] Further, even in the cubic phase, near the metal-insulator transition, the resistivity in the normal state shows evidence of nonmetallic behavior above the superconducting transition.[12]

The behavior of $Ba_{1-x}K_xBiO_3$ is similar to that of the $BaPb_{1-x}Bi_xO_3$ system, where superconductivity also occurs near a metal-insulator transition associated with a structural phase transition.[14] Since the discovery of superconductivity in the $BaPb_{1-x}Bi_xO_3$ system, there have been many proposals to account for the metal-insulator transition. However, there is still no agreement on the cause of the Fermi surface gap in the heavily doped semiconducting phase.[15-22] According to a simple electron-band theory, the parent material, $BaBiO_3$, has an exactly half-filled band, and, in principle, a 6*s* electron on every Bi atom, leading to Bi^{4+} and metallic behavior. However, the valence state Bi^{4+} is always unfavorable due to correlation energies on the Bi atoms. Thus, the electronic system is unstable to the formation of either antifer-

romagnetism or charge-density waves (CDW) that create an insulating gap at the Fermi surface. Neutron-diffraction studies[15,16] have shown that oxygen breathing-mode distortions indeed exist in $BaBiO_3$, giving rise to an ordered arrangement of Bi^{3+} and Bi^{5+} ions (i.e., a commensurate CDW), and, therefore, explain the semiconducting behavior in $BaBiO_3$. However, this commensurate CDW disappears rapidly on Pb substitution.[17] It is not possible to create, in the context of local-density-functional-based band theory, an insulating gap from $Bi(Pb)O_6$ octahedral tilts in the absence of the breathing-mode distortions. To address this problem, many theories have been proposed attributing the semiconducting behavior of the Pb-substituted compound to a local CDW,[19] chemical ordering wave,[20] or long-range incommensurate CDW.[21] Since such postulated structural features have not been established experimentally, the semiconducting behavior of the $BaPb_{1-x}Bi_xO_3$ (and now the $Ba_{1-x}K_xBiO_3$) system is still an intriguing problem.

The purpose of the present work was to investigate, with neutron powder diffraction, the structural phase diagram of the $Ba_{1-x}K_xBiO_3$ system over a wide range of composition, x, and temperature, and to look for evidence of commensurate or incommensurate CDW instabilities. Although the cubic symmetry of the superconducting phase has been confirmed in several laboratories[2,3,23-26] (Fig. 1), and the body-centered monoclinic, $I2/m$, structure of the parent phase, $BaBiO_3$, has been known for a number of years,[15,16,27-29] few details have been reported about the other structures that exist as a function of potassium composition and temperature. Moreover, the work that has been reported often conflicts. Hinks *et al.*[3] showed, by neutron powder diffraction, that adjacent to the primitive cubic, superconducting phase ($x<0.4$, starting composition) the cubic cell transforms to a $\sqrt{2}a_p\times\sqrt{2}a_p\times 2a_p$ supercell (where a_p is the edge of the primitive pseudocubic cell). However, Wignacourt *et al.*[30] did not detect any supercell reflections in a single-crystal x-ray diffraction study and reported a cubic structure for $x=0.13$ at room temperature. At $x=0.04$, Schneemeyer *et al.*,[31] using single-crystal x-ray diffraction, observed a $\sqrt{2}a_p\times\sqrt{2}a_p\times 2a_p$ supercell phase with *Immm* symmetry.

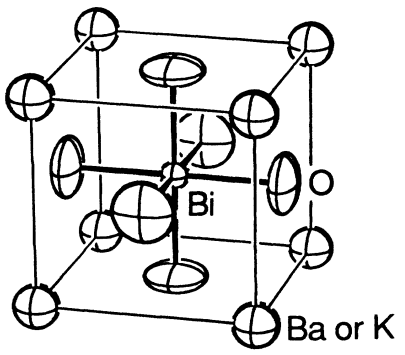

FIG. 1. The structure of cubic $Ba_{1-x}K_xBiO_3$ ($x\geq 0.37$).

In addition to the commensurate supercell structures, an incommensurate structural modulation may also occur in the $Ba_{1-x}K_xBiO_3$ system. Pei *et al.*[26] observed, by electron diffraction, an incommensurate modulation along the [110] cubic direction in the nonsuperconducting supercell phase. They speculated that such a modulation could be responsible for the semiconducting behavior in the supercell phase. Hewat *et al.*[32] also observed this incommensurate modulation, but concluded that it was included by the electron beam. Neither group provided a clear microscopic explanation for the modulation, although Hewat *et al.*[32] concluded that it did not result from the ordering of oxygen vacancies or potassium substitutional defects.

II. SAMPLE PREPARATION AND CHARACTERIZATION

For the present experiments, a series of $Ba_{1-x}K_xBiO_3$ samples with $0.1\leq x\leq 0.6$ was prepared using the two-step synthesis method previously described.[3,33] Stoichiometric mixtures of Bi_2O_3, BaO, and KO_2 powders were first heated to 725° (at 2 °C/m) in flowing nitrogen, held at 725 °C for 1 h, and cooled to room temperature. The samples were then heated to 425 °C (at 2 °C/m) in flowing oxygen, held for 1 h, and cooled to room temperature. This two-step procedure was repeated several times, with intermediate grinding to improve sample homogeneity. For this synthesis procedure, we found a solubility limit for potassium near $x=0.5$. The $BaBiO_3$ sample was made by directly melting a stoichiometric mixture of Bi_2O_3 and BaO powders. The oxygen content of these samples was not measured independently, but from previous work[33] it is known that samples made in this way are fully oxygenated. Additionally, for the superconducting compositions the measured T_c's are a confirmation of this conclusion, since T_c is known to decrease sharply when oxygen vacancies are present.[3,12]

Superconducting transition temperatures, T_c, of these samples were measured resistively. The Meissner effect and diamagnetic shielding have been measured previously for samples made by the same technique.[34] The resistively measured T_c's for the present samples are shown in Fig. 2. Sharp resistive transitions were observed for $0.35\leq x\leq 0.45$. For $0.3\leq x<0.35$, resistive onsets were observed but zero resistance was not achieved at any temperature above 10 K. Samples with $x<0.3$ were semiconducting. The previous diamagnetic shielding measurements showed that, even though resistive transitions are observed for values of x as low as 0.3, the fraction of superconducting phase decreases sharply for $x<0.37$.[34] As shown in Fig. 2, this is the same composition where T_c begins decreasing with increasing x. Thus, we conclude that bulk superconductivity occurs only for $x\geq 0.37$ and that T_c decreases with increasing x as shown in Fig. 2. We attribute the apparent smearing of the boundary between the superconducting and nonsuperconducting phases, which leads to constant resistive onset

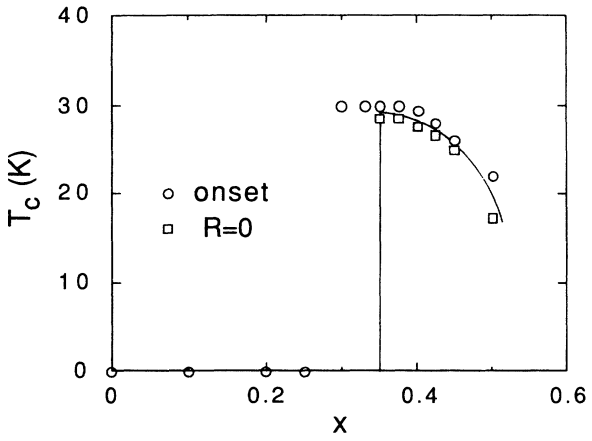

FIG. 2. Superconducting transition temperatures T_c vs x for $Ba_{1-x}K_xBiO_3$. Circles mark the resistive onset temperatures and squares mark the zero-resistance temperatures. Where no square symbols are shown, zero resistance was not reached at any temperature above 10 K.

temperatures but a rapidly changing superconducting fraction for $0.3 \leq x < 0.37$, to difficulties in achieving sample homogeneity. The superconducting transition also broadens at $x=0.5$, where the solubility limit for potassium is reached.

III. NEUTRON POWDER DIFFRACTION

Neutron powder diffraction data were collected using the H4S triple-axis spectrometer at the Brookhaven High Flux Reactor and the Special Environment Powder Diffractometer (SEPD) at Argonne's Intense Pulsed Neutron Source.[35] These instruments are complementary for this study. The constant-wavelength method using H4S offers the low background needed to search for incommensurate Bragg peaks and the ability to efficiently measure the temperature dependence of selected superlattice reflections, while the SEPD time-of-flight diffractometer provides complete data covering a wide range of d spacings suitable for Rietveld refinements[36] of the structures. At Brookhaven, the samples were sealed in thin-walled aluminum cans with helium-exchange gas and were cooled with a close-cycle helium (Displex) refrigerator (10–300 K). A wavelength of 2.3701 Å was selected from the (002) plane of a pyrolytic graphite monochromator. Data were collected in 0.1° steps. At Argonne, the samples were sealed in thin-walled vanadium cans with helium-exchange gas. The temperature of the samples was controlled using either a close-cycle helium (Displex) refrigerator (10–300 K), or a simple radiantly heated furnace (300–473 K). On the SEPD, time-of-flight data are collected simultaneously at several different scattering angles. However, only the high-resolution back-scattering data ($\Delta d/d \approx 0.0035$ at $2\theta = 150°$) were used for full structural analyses by Rietveld refinement.[36]

The first data were collected at Brookhaven, from an initial set of samples with $x=0$, 0.1, 0.2, 0.3, and 0.4. Although these samples showed some evidence for oxygen deficiency and inhomogeneity, these early data provided a clear picture of the growth of the weak superlattice reflections as a function of temperature and composition, and allowed possible space groups for the various phases to be identified. Later data were collected on the SEPD using an improved set of samples with $x=0$, 0.1, 0.2, 0.25, 0.3, 0.35, 0.4, 0.5, and 0.6. The SEPD data were used to refine the structures and establish the structural phase diagram.

IV. CRYSTAL STRUCTURES AND PHASE DIAGRAM

The structures that occur in the $Ba_{1-x}K_xBiO_3$ system can be viewed as distortions of the basic cubic perovskite structure shown in Fig. 1. The fundamental distortions are tilts of the nominally rigid BiO_6 octahedra and breathing-mode distortions in which alternating Bi sites become inequivalent because of oxygen-atom displacements toward or away from the Bi atoms. These tilting and breathing-mode distortions can occur singly or in combination to produce various possible distorted perovskite structures. Glazer has classified those structures created by octahedral tilts around one, two, or three axes with repeat periods of up to two cubic-cell constants.[37,38] Although this classification scheme is based on rigid tilts, many of the resulting space groups include degrees of freedom that also allow (or require) distortions of the BiO_6 octahedra. Moreover, space groups that allow breathing-mode distortions can be derived from

TABLE I. Possible space groups resulting from negative tilts of BiO_6 octahedral (Refs. 37 and 38). The axes and planes are designated in terms of the primitive pseudocubic cell with an edge of a_p.

Tilt system	Special tilt axis	Cell dimensions	Space group
$a^-b^-c^-$	not unique	$2a_p \times 2a_p \times 2a_p$	$P\bar{1}$ (no. 2)[a]
$a^-b^-b^-$	on $(011)_p$ plane	$\sqrt{2}a_p \times \sqrt{2}a_p \times 2a_p$	$I2/a$ (no. 15)
$a^-a^-a^-$	$[111]_p$	$2a_p \times 2a_p \times 2a_p$	$R\bar{3}c$ (no. 167)[a]
$a^0b^-c^-$	on $(100)_p$ plane	$2a_p \times 2a_p \times 2a_p$	$I2/m$ (no. 12)
$a^-a^-c^0$	$[110]_p$	$\sqrt{2}a_p \times \sqrt{2}a_p \times 2a_p$	$Ibmm$ (no. 74)
$a^0a^0c^-$	$[001]_p$	$\sqrt{2}a_p \times \sqrt{2}a_p \times 2a_p$	$I4/mcm$ (no. 14)

[a]This space group refers to the smaller primative unit cell equivalent to the F-centered one.

Glazer's scheme by appropriate reductions of symmetry. Although Glazer's classification scheme does not include all possible distorted perovskite structures, it has been widely used to identify distorted perovskite structures and to understand the associated phase transitions. In particular, this strategy was successful in identifying structures in the closely related $BaPb_{1-x}Bi_xO_3$ system.[15–17] Therefore, we have used the same approach to investigate the structures of $Ba_{1-x}K_xBiO_3$.

With the exception of the data for $x=0$ at low temperature (discussed later) all of the observed supercell reflections in our data can be indexed in terms of the primitive cubic cell with odd half-integer indices. In Glazer's tilt scheme,[37,38] this suggests that only negative octahedral tilts are allowed. The corresponding space groups are listed in Table I.

Other than the $BaBiO_3$ phase, whose monoclinic structure is already known,[15,16,27–29] we found no evidence in our data to adopt low-symmetry triclinic or monoclinic structures that result from tilts along the nonprincipal axes, i.e., $a^-b^-c^-$, $a^-b^-b^-$, and $a^0b^-c^-$. Thus, only tilts along the three major axes, i.e., $[111]_p$, $[110]_p$, and $[001]_p$ (where the subscript p refers to the primitive cubic, perovskite cell) were considered. When these three tilts are combined with breathing-mode distortions, eight possible space groups, including two with no tilts (i.e., $Pm\bar{3}m$ and $Fm\bar{3}m$), result (Table II), of which $I4/mcm$, $I2/m$, $Ibmm$, and $R\bar{3}$ have been observed by Cox and Sleight in the $BaPb_{1-x}Bi_xO_3$ system.[15–17]

Figure 3 shows the temperatures and sample compositions for which full Rietveld refinements of data from the SEPD were performed, and the corresponding structural phase boundaries. Table III summarizes the crystallographic information derived from these refinements. Five different phases were observed at potassium concentrations below $x=0.5$ and at temperatures below 473 K. Each of the phases will be discussed in detail.

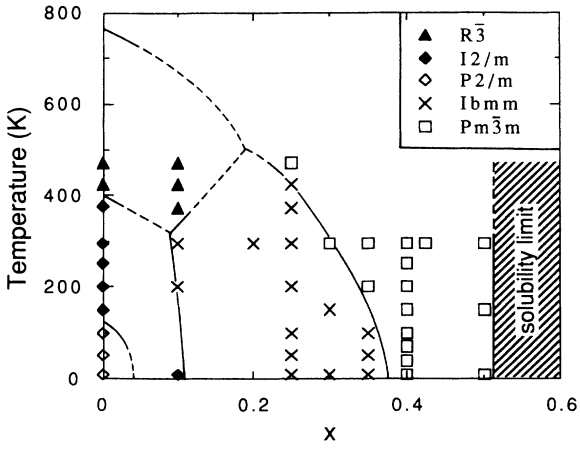

FIG. 3. Phases identified by neutron powder diffraction in the $Ba_{1-x}K_xBiO_3$ ($x \leq 0.5$) system. Each symbol marks a composition and temperature for which a Rietveld structural refinement has been performed. The exact location of the phase boundaries is limited by the number of data.

TABLE II. Possible space groups resulting from combinations of negative BiO_6 octahedral tilts and breathing-mode oxygen-atom displacements. The tilt axes are designated in terms of the primitive pseudocubic cell with an edge of a_p. Expressions for the average tilt angle ϕ and the difference between the average Bi—O distances of two distinct Bi sites Δr are given in terms of the oxygen-atom coordinates. Bi atoms are located at (0,0,0) and $(\frac{1}{2},0,0)$ in $Fm\bar{3}m$, at (0,0,0) and $(\frac{1}{2},\frac{1}{2},\frac{1}{2})$ in the rhombohedral groups, and at (0,0,0) and $(0,0,\frac{1}{2})$ in the tetragonal, orthorhombic, and monoclinic groups. Oxygen atoms are located at $(x,0,0)$ with $x \approx \frac{1}{4}$ in $Fm\bar{3}m$, at (x,y,x) with $-x \approx y \approx z \approx \frac{1}{4}$ in the rhombohedral groups, and at (x_1,y_1,z_1) with $x_1 \approx 0$, $y_1 = 0$, and $z_1 \approx \frac{1}{4}$ and at (x_2,y_2,z_2) with $x_2 \approx y_2 \approx \frac{1}{4}$ and $z_2 \approx 0$ in the tetragonal, orthorhombic, and monoclinic groups. a, b, c are the edges of the unit cells and α ($\sim 60°$) is the angle between two rhombohedral axes.

	No tilt	$[001]_p$	$[110]_p$	$[111]_p$
Tilt only				
Space group	$Pm\bar{3}m$ (no. 221)	$I4/mcm$ (no. 140)	$Ibmm$ (no. 74)	$R\bar{3}c$ (no. 167)
Cell dimensions (Å^3)	$(a_p)^3$	$\sqrt{2}a_p \times \sqrt{2}a_p \times 2a_p$	$\sqrt{2}a_p \times \sqrt{2}a_p \times 2a_p$	$(\sqrt{2}a_p)^3 \times (1-3\cos^2\alpha+2\cos^3\alpha)^{1/2}$
ϕ (rad)	0	$1-4x_2$	$\frac{1}{3}(4x_1a/c-8z_2c/a)$	$\sqrt{2}(\frac{1}{2}-2y)$
Tilt + breathing				
Space group	$Fm\bar{3}m$ (no. 225)	$I4/m$ (no. 87)	$I2/m$ (no. 12)	$R\bar{3}$ (no. 148)
Cell dimensions (Å^3)	$(2a_p)^3$	$\sqrt{2}a_p \times \sqrt{2}a_p \times 2a_p$	$\sqrt{2}a_p \times \sqrt{2}a_p \times 2a_p$	$(\sqrt{2}a_p)^3 \times (1-3\cos^2\alpha+2\cos^3\alpha)^{1/2}$
ϕ (rad)	0	$2(x_2-y_2)$	$\frac{1}{3}(4x_1a/c-8z_2c/a)$	$\sqrt{3}(z-y)$
Δr (Å)	$2(x-\frac{1}{4})a$	$\frac{2}{3}[(z_1-\frac{1}{4})c+\sqrt{2}(x_2+y_2-\frac{1}{2})a]$	$\frac{2}{3}\{(z_1-\frac{1}{4})c+\sqrt{2}[(x_2-\frac{1}{4})a+(y_2-\frac{1}{4})b]\}$	$\sqrt{2}(y+z-\frac{1}{2})a$

A. Cubic phase

The superconducting phase has an undistorted cubic perovskite structure. The oxygen octahedra are identical and perfectly regular with no tilts. Samples with $x=0.4$ and 0.5 were cubic at all temperatures from 10 to 295 K in agreement with other published results.[2,3,23–26] For $x=0.35$, a transition to the orthorthombic phase occurs between 200 and 100 K. From this we conclude that the transition between the cubic and orthorhombic phases occurs near $x=0.37$ at low temperatures and, thus, corresponds to the onset of bulk superconductivity.

It should be noted that this value of x for the onset of superconductivity differs from that reported in our previously work.[3] In our first study we assumed that a net loss of potassium from the sample could occur and, thus, assigned the value of x in the $Ba_{1-x}K_xBiO_3$ phase based on the Rietveld refinement. Thermogravimetric analysis (TGA) measurements show that the net loss of potassium from the sample is negligible, and that the starting compositions should be taken as the correct values if single-

TABLE III. Refined lattice parameters in the $Ba_{1-x}K_xBiO_3$ system. β ($\sim 90°$) and α ($\sim 60°$) are, respectively, the monoclinic angle and the angle between trigonal axes. Numbers in parentheses are the estimated standard deviations of the last significant digit.

x	T (K)	Space group	a (Å)	b (Å)	c (Å)	β/α (deg)
0	473	$R\bar{3}$	6.1521(1)			60.271(2)
	423	$R\bar{3}$	6.1469(1)			60.300(2)
	379	$I2/m$	6.1864(2)	6.1459(1)	8.6821(2)	90.130(3)
	295	$I2/m$	6.1863(1)	6.1406(1)	8.6723(1)	90.164(2)
	250	$I2/m$	6.1855(1)	6.1364(1)	8.6656(1)	90.190(2)
	200	$I2/m$	6.1844(1)	6.1323(1)	8.6591(1)	90.221(2)
	150	$I2/m$	6.1834(1)	6.1285(1)	8.6531(1)	90.250(2)
	100	$P2/m$	6.1802(1)	6.1257(1)	8.6508(1)	90.258(2)
	50	$P2/m$	6.1764(1)	6.1246(1)	8.6503(1)	90.257(2)
	10	$P2/m$	6.1752(1)	6.1242(1)	8.6505(1)	90.254(2)
0.1	473	$R\bar{3}$	6.1424(1)			60.143(3)
	423	$R\bar{3}$	6.1366(1)			60.175(3)
	373	$R\bar{3}$	6.1319(1)			60.191(3)
	295	$Ibmm$	6.1578(2)	6.1262(2)	8.6569(2)	
	200	$Ibmm$	6.1568(2)	6.1190(2)	8.6415(2)	
	10	$I2/m$	6.1551(1)	6.1088(1)	8.6256(2)	90.077(9)
0.2	295	$Ibmm$	6.1280(5)	6.1040(4)	8.6286(6)	
0.25	295	$Ibmm$	6.1118(9)	6.0926(6)	8.6133(10)	
	200	$Ibmm$	6.1062(9)	6.0873(6)	8.6038(9)	
	10	$Ibmm$	6.0975(16)	6.0856(13)	8.5839(14)	
0.3	295	$Pm\bar{3}m$	4.3006(1)			
	150	$Ibmm$	6.0795(3)	6.0767(5)	8.5867(9)	
	10	$Ibmm$	6.0691(5)	6.0625(6)	8.6050(4)	
0.35	295	$Pm\bar{3}m$	4.2953(1)			
	10	$Ibmm$	6.0664(2)	$=a$	8.5670(7)	
0.4	295	$Pm\bar{3}m$	4.2830(1)			
	250	$Pm\bar{3}m$	4.2811(1)			
	200	$Pm\bar{3}m$	4.2791(1)			
	150	$Pm\bar{3}m$	4.2771(1)			
	100	$Pm\bar{3}m$	4.2756(1)			
	50	$Pm\bar{3}m$	4.2744(1)			
	10	$Pm\bar{3}m$	4.2742(1)			
0.425	295	$Pm\bar{3}m$	4.2789(1)			
0.5	295	$Pm\bar{3}m$	4.2698(1)			
	150	$Pm\bar{3}m$	4.2642(1)			
	10	$Pm\bar{3}m$	4.2618(1)			

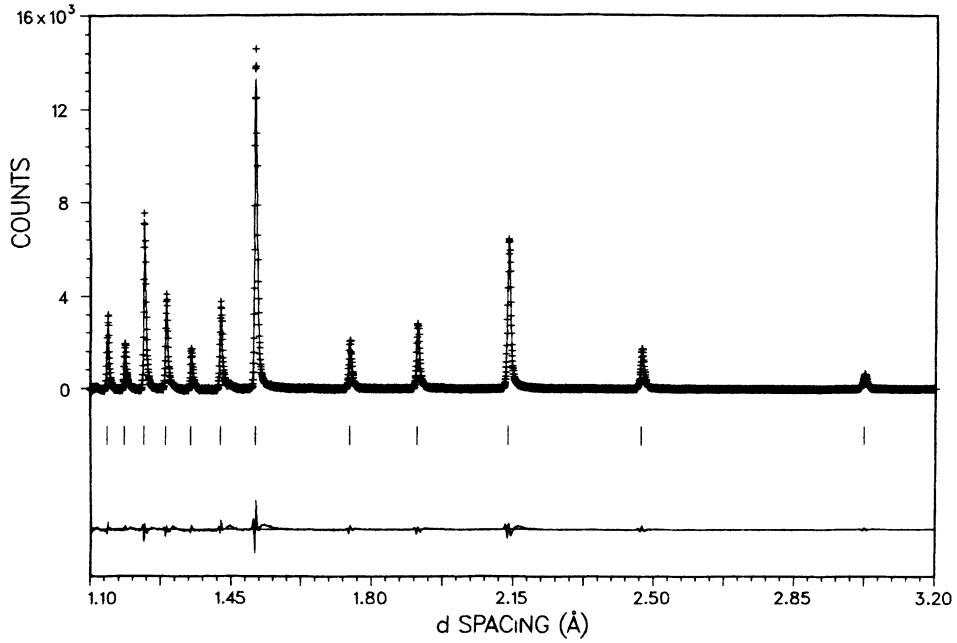

FIG. 4. Portion of the Rietveld refinement profile for cubic ($Pm\bar{3}m$) $Ba_{0.6}K_{0.4}BiO_3$ at 10 K. Plus marks (+) are the raw data. The solid line is the calculated profile. Tick marks below the profile mark the positions of allowed reflections. A difference curve (observed minus calculated) is plotted at the bottom. Background has been fit as part of the refinement but subtracted prior to plotting.

phase samples are formed.[33] Self-consistent results for the various phases in the $Ba_{1-x}K_xBiO_3$ system, including the $x=0$ phase, can be obtained if a scattering length of $b=0.55\times10^{-12}$ cm is assigned to Ba [compared to the literature value of $b=0.525\times10^{-12}$ cm (Ref. 39)] or if the Bi scattering length is decreased by a similar amount. It is unlikely that the scattering lengths for normal abundance Ba or Bi are in error. Rather, we conclude that this small discrepancy results from a systematic error in the data or from random nonharmonic atomic displacements around the substitutional defects (or associated with the incommensurate modulation that will be discussed later) that are not included in the structural model.

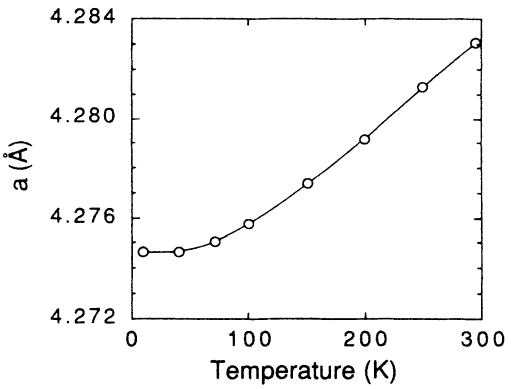

FIG. 5. Lattice parameter a for cubic $Ba_{0.6}K_{0.4}BiO_3$ vs temperature.

Figure 4 shows the Rietveld refinement profile at 10 K for the $x=0.4$ sample. The refined structural parameters at 295 and 10 K are given in Table IV. A pronounced anisotropy in the oxygen vibration, with the largest dis-

TABLE IV. Refined structural parameters for $Ba_{0.6}K_{0.4}BiO_3$ at 295 and 10 K. The data were refined in the cubic $Pm\bar{3}m$ space group. Numbers in parentheses are estimated standard deviations of the last significant digit. Where no standard deviation is given, the parameter was not refined.

		295 K	10 K
a (Å)		4.2830(1)	4.2742(1)
Ba	$x=y=z$	0	0
	B (Å^2)	0.99(3)	0.44(3)
	n	0.58(2)	0.57(2)
K	n	$=1-n$(Ba)	$=1-n$(Ba)
Bi	$x=y=z$	$\frac{1}{2}$	$\frac{1}{2}$
	B (Å^2)	0.38(2)	0.18(2)
	n	1	1
O	$x=y$	$\frac{1}{2}$	$\frac{1}{2}$
	z	0	0
	$U_{11}=U_{22}$ (Å^2)	0.0248(3)	0.0164(3)
	U_{33} (Å^2)	0.0058(4)	0.0039(4)
	n	3	3
R_{wp} (%)		7.34	8.57
R_{exp} (%)		3.70	3.73

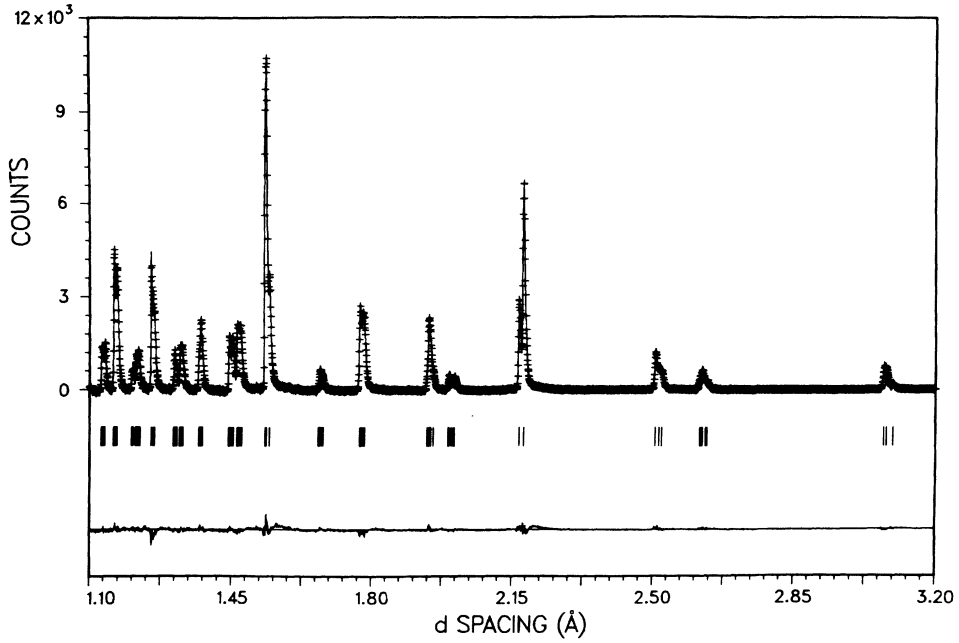

FIG. 6. Portion of the Rietveld refinement profile for body-centered monoclinic ($I2/m$) $BaBiO_3$ at 295 K. The format is the same as Fig. 4.

placement perpendicular to the Bi—O—Bi bond, is evident at both temperatures. This is consistent with a tendency towards a rotational phase transition. The variation in the cubic-lattice parameter with temperature is shown in Fig. 5. The thermal expansion has the expected behavior, becoming small at the lowest temperatures.

At lower potassium contents, the cubic phase is stable at higher temperatures. In the SEPD data, we observed the cubic phase at 295 K for $x=0.3$ and at 473 K for $x=0.25$. When combined with the data of Cox and Sleight,[16] who observed a transition to cubic symmetry in $BaBiO_3$ between 750 and 800 K, these results suggest that the cubic phase is the stable phase at high temperature for all compositions and lead to the phase boundary as shown in Fig. 3. It should be noted that the phase diagram has not been investigated above 473 K for $x>0$. At high temperature the presence of oxygen vacancies could alter the phase boundaries. Thermogravimetric analysis shows that loss of oxygen from $Ba_{1-x}K_xBiO_3$ begins at temperatures above 600 K and depends on the value of x.[40] Thus, over the temperature range that we have investigated, the oxygen content is stoichiometric.

B. Body-centered monoclinic phase

The end-member phase has the body-centered monoclinic, $I2/m$, structure of $BaBiO_3$.[15,16,27–29] This structure consists of an octahedral tilt (along the $[110]_p$ axis) and distortion produced by breathing-mode oxygen atom displacements. This breathing-mode distortion creates two distinct Bi sites, giving rise to the bismuth charge disproportionation (or a commensurate CDW) discussed by Cox and Sleight,[15,16] and Thornton and Jacobsen,[27] and results in semiconducting behavior.

We observe the $I2/m$ structure for $x=0$ at temperatures from 150 to 379 K and also for $x=0.1$ at 10 K as shown in Fig. 3. For $x=0.1$ at higher temperatures, an orthorhombic structure is observed. The Rietveld

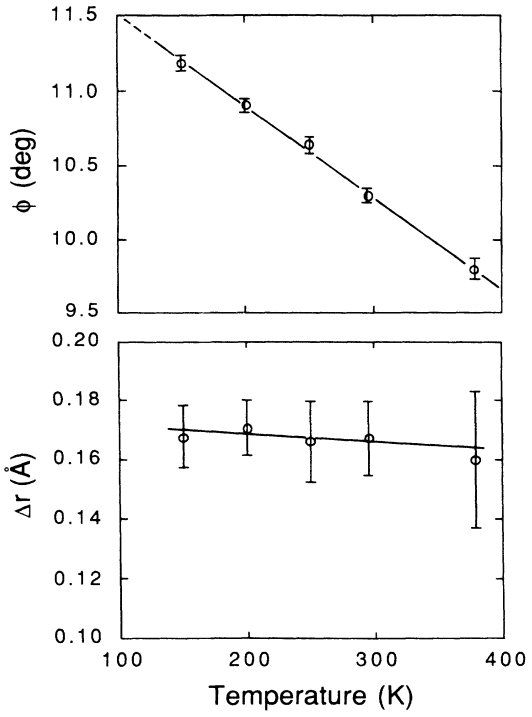

FIG. 7. Average rotation angle ϕ and the difference between the averaged Bi—O distances for the two distinct Bi atoms Δr for monoclinic ($I2/m$) $BaBiO_3$ vs temperature. Here, ϕ is the tilt angle with respect to the pseudocubic [110] axis.

refinement profile of the SEPD data for $BaBiO_3$ at 295 K is shown in Fig. 6. The values of the refined parameters for $x=0$ at 295 K and $x=0.1$ at 10 K are given in Table V. Our results agree well with previously published data.[15,16,27–29] For $x=0$ at 295 K the octahedral tilt is nearly rigid, with an average tilt angle of 10.3°. The six oxygen atom neighbors around one Bi atom are closer than those around the neighboring Bi atom by 0.17 Å. The refined monoclinic angle β is 90.164°, the difference from 90° reflecting the fact that the two adjacent octahedra along the c-axis direction are not of identical size, and consequently their $[110]_p$ tilting cannot be fully canceled.

The variations of the tilt angle and the breathing-mode distortion for $x=0$ with temperature are shown in Fig. 7.

TABLE V. Refined structural parameters for monoclinic $BaBiO_3$ at 295 K and $Ba_{0.9}K_{0.1}BiO_3$ at 10 K. The data were refined in the monoclinic $I2/m$ space group. Numbers in parentheses are estimated standard deviations of the last significant digit. Where no standard deviation is given, the parameter was not refined.

		$x=0$ 295 K	$x=0.1$ 10 K
a (Å)		6.1908(1)	6.1551(1)
b (Å)		6.1450(1)	6.1088(1)
c (Å)		8.6785(1)	8.6256(2)
β (deg)		90.164(2)	90.077(9)
Ba	x	0.5029(6)	0.5062(5)
	y	0	0
	z	0.2487(8)	0.25
	B (Å^2)	1.08(4)	0.46(2)
	n	1.01(1)	0.93(2)
K	n	0	$=1-n$(Ba)
Bi(1)	$x=y=z$	0	0
	B (Å^2)	0.49(5)	0.00
	n	0.5	0.5
Bi(2)	$x=y$	0	0
	z	$\frac{1}{2}$	$\frac{1}{2}$
	B (Å^2)	0.06(4)	$=B$[Bi(1)]
	n	0.5	0.5
O(1)	x	0.0606(4)	0.0587(4)
	y	0	0
	z	0.2604(5)	0.253(1)
	U_{11} (Å^2)	0.019(1)	$B=0.62(4)$
	U_{22} (Å^2)	0.035(2)	
	U_{33} (Å^2)	0.006(2)	
	n	1	1
O(2)	x	0.2611(6)	0.253(1)
	y	0.2574(8)	$=x$[O(2)]
	z	−0.0327(3)	−0.0315(2)
	U_{11} (Å^2)	0.021(2)	$B=1.03(3)$
	U_{22} (Å^2)	0.019(2)	
	U_{33} (Å^2)	0.024(2)	
	U_{12} (Å^2)	−0.014(1)	
	n	2	2
R_{wp} (%)		5.51	7.01
R_{exp} (%)		4.04	3.50

The tilt angle increases with decreasing temperature, while the breathing-mode distortion remains approximately constant. The dependence on potassium content x is more dramatic. A small monoclinic distortion ($\beta=90.08°$) is observed for the $x=0.1$ sample at 10 K. Here, the tilt angle is reduced only slightly to 9.9° while the difference in Bi—O bond lengths is reduced markedly to 0.05 Å. It would be expected that a further small increase in potassium content should fully suppress the breathing-mode oxygen atom displacements while allowing a nonzero octahedral tilt, consistent with the observed *Ibmm* orthorhombic structure (see Fig. 3 and below). Conversely, elimination of the tilting distortion while maintaining the breathing-mode distortion would lead to a $2a_p\times2a_p\times2a_p$ cubic $Fm\bar{3}m$ structure, which we have not observed in this system.

C. Orthorhombic phase

Only one phase is observed in the region between the monoclinic and cubic phases. The structure of this phase has been identified as orthorhombic with space group *Ibmm*. This structure contains the same $[110]_p$ octahedral tilt as the $I2/m$ phase but has no breathing-mode distortion, and is a logical intermediate structure between the monoclinic $I2/m$ and cubic $Pm\bar{3}m$ phases.

The identification of this structure is based on the comparison of Rietveld refinements using the *Ibmm* space group with refinements using other possible space groups listed in Table II. As described in our original paper,[3] superlattice reflections that can be indexed on a body-centered $\sqrt{2}a_p\times\sqrt{2}a_p\times2a_p$ supercell are clearly visible in the raw neutron-diffraction data, but no tetragonal or orhorhombic strain was evident with the available instrumental resolution for the composition originally studied ($x=0.2$, starting composition). This difficulty in directly determining the cell symmetry allows a number of tetragonal, orthorhombic, and face-centered-cubic ($2a_p\times2a_p\times2a_p$) unit cells, all of which are consistent with the observed superlattice reflections. Fortunately, in the present data, a nonzero orthorhombic strain is observed for $x=0.1$ at 295 K and a sufficiently large number of superlattice peak intensities are measured to allow R-value ratio tests[41] to be used to differentiate between the various space groups which obey the observed selection rules. (The appropriate R values for time-of-flight Rietveld refinement are defined in Ref. 36.) In this way, the *Ibmm* space group was clearly established for $x=0.1$ at 295 K and the same model was then applied to the data for other compositions and temperatures. The Rietveld refinement profile for $x=0.1$ at 295 K is shown in Fig. 8 and the values of refined parameters for $x=0.1$ and 0.2 at 295 K are given in Table VI.

Schneemeyer *et al.*[31] have reported an orthorhombic *Immm* structure for a single crystal of composition $Ba_{0.96}K_{0.04}BiO_3$. This structure contains an asymmetric breathing-mode distortion with no octahedral tilt. The asymmetric breathing-mode distortion is qualitatively different from the symmetric breathing-mode distortion present in the $I2/m$ structure. In the asymmetric case, four of the six Bi—O bonds are lengthened (or shortened,

for the adjacent Bi atom) while the other two are shortened (or lengthened); in the symmetric case, all six bonds are lengthened (or shortened). The superlattice peak intensities in the neutron-diffraction case are a sensitive probe of these local atom displacements. The *Immm* model was strongly rejected by *R*-value ratio tests[41] for all of our data in the orthorhombic phase. For example, for $x=0.1$ at 295 K, the respective weighted profile *R* values (defined in Ref. 36) were $R_{wp}(Ibmm)=7.81\%$ and $R_{wp}(Immm)=10.21\%$. Since we have no data for $x=0.04$, we are unable to determine whether the *Immm* structure exists for some composition between $x=0$ and 0.1. However, based on the systematic evolution of the tilting and breathing-mode distortions we have observed in the present work, we consider it unlikely that the *I*2/*m* and *Ibmm* phases are separated by a phase of *Immm* symmetry.

Although the identification of the *Ibmm* structure at $x=0.1$ and 295 K is clear, it is important to determine whether a second phase transition, to yet another structure consistent with the observed supercell peaks, occurs at low temperature or with increasing *x* between the orthorhombic and the cubic phases. Clearly, as the orthorhombic strain drops below the limit of detectability imposed by instrumental resolution and intrinsic sample peak broadening, the occurrence of additional subtle phase transitions is difficult to completely rule out. Thus, refinements of the $x>0.1$ data in other possible space groups listed in Table II were attempted for comparison with the *Ibmm* refinements.

The $R\bar{3}c$ structure contains a rigid octahedral tilt around the $[111]_p$ axis, with no breathing-mode distortion. This structure was immediately rejected, based on a

TABLE VI. Refined structural parameters for $Ba_{1-x}K_xBiO_3$, $x=0.1$ and 0.2, at 295 K. The data were refined in the orthorhombic *Ibmm* space group. Numbers in parentheses are estimated standard deviations of the last significant digit. Where no standard deviation is given, the parameter was not refined.

		$x=0.1$	$x=0.2$
a (Å)		6.1578(2)	6.1280(5)
b (Å)		6.1262(2)	6.1040(4)
c (Å)		8.6569(2)	8.6286(6)
Ba	*x*	0.504(1)	0.507(2)
	y	0	0
	z	$\frac{1}{4}$	$\frac{1}{4}$
	B (Å^2)	1.14(3)	0.91(4)
	n	0.90(2)	0.80(2)
K	*n*	$1-n$(Ba)	$1-n$(Ba)
Bi	$x=y=z$	0	0
	B (Å^2)	0.42(2)	0.27(3)
	n	1	1
O(1)	*x*	0.0527(6)	0.047(1)
	y	0	0
	z	$\frac{1}{4}$	$\frac{1}{4}$
	B (Å^2)	1.33(6)	1.01(8)
	n	1	1
O(2)	*x*	$\frac{1}{4}$	$\frac{1}{4}$
	y	$\frac{1}{4}$	$\frac{1}{4}$
	z	−0.0265(3)	−0.0116(7)
	B (Å^2)	2.07(5)	2.04(7)
	n	2	2
R_{wp} (%)		7.81	9.63
R_{exp} (%)		3.38	3.29

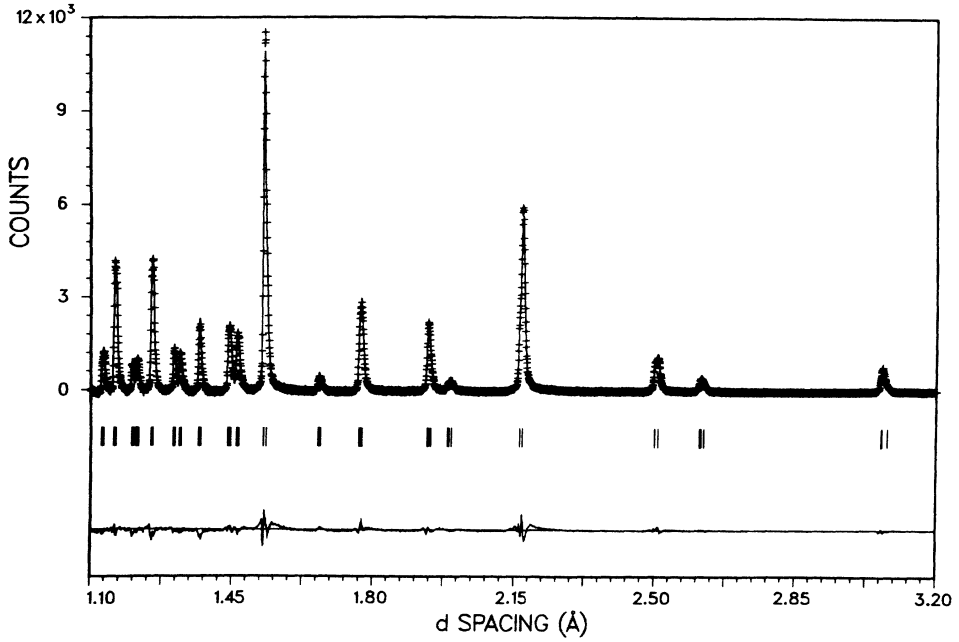

FIG. 8. Portion of the Rietveld refinement profile for orthorhombic (*Ibmm*) $Ba_{0.9}K_{0.1}BiO_3$ at 295 K. The format is the same as Fig. 4.

large difference in R values, when compared to the *Ibmm* model. The $R\bar{3}$ structure, which exists for $x \leq 0.1$ at elevated temperature (see Fig. 3 and below), was also rejected based on R-value ratio tests.[41]

The $Fm\bar{3}m$ cubic phase, with cell dimensions $2a_p \times 2a_p \times 2a_p$, is consistent with the lack of observable tetragonal or orthorhombic strain as the transition to the simple-cubic phase is approached. This phase contains a symmetric breathing-mode distortion with no octahedral tilt. Attempted Rietveld refinements, however, yielded large discrepancies for the fitted peak intensities, allowing this phase to also be rejected.

The $I4/m$ structure contains the combination of a $[001]_p$ octahedral tilt and a breathing-mode distortion. Refinements based on this model, however, are found to be unstable with respect to the oxygen positions. Considering further the fact that breathing-mode distortions have already vanished near $x=0.1$, it appears highly unlikely that this $I4/m$ structure would be present at higher potassium contents.

The tetragonal, $I4/mcm$ structure, having a rigid octahedral tilt around the $[001]_p$ axis and no breathing-mode distortion, falls in a logical sequence of phase transitions, $I2/m \rightarrow Ibmm \rightarrow I4/mcm \rightarrow Pm\bar{3}m$, involving first the loss of the breathing-mode distortion and then the successive loss of octahedral tilts. Equivalently, the $I4/mcm$ phase can be viewed as resulting from the condensation of one rotational phonon mode while the *Ibmm* phase results from the condensation of two degenerate rotational phonon modes. R-value ratio tests,[41] however, favor the *Ibmm* structure over the $I4/mcm$ structure for all of the compositions and temperatures for which we presently have data. The R-value ratio is large for regions of the phase diagram far from the cubic phase and decreases somewhat for increasing x. For example, at 295 K, $R_{wp}(I4/mcm)/R_{wp}(Ibmm)=1.290$ for $x=0.1$ and 1.056 for $x=0.2$. In addition, the c-axis expansion as observed at the *Ibmm*-$I4/mcm$ transition in $BaPb_{1-x}Bi_xO_3$ (Ref. 17) is not present in this system; we observe only a continuous variation of the c axis into the cubic phase (Fig. 9). It is also instructive to plot the order parameter associated with the orthorhombic strain, $(a-b)^2$, as a function of x and compare it with the order parameter associated with the octahedral tilting angle ϕ^2 as shown in Fig. 10. The strain and tilt parameters scale together near the orthorhombic-cubic transition ($x=0.3$ at 295 K), and both exibit the expected mean-field behavior for a continuous transition from the orthorhombic to the cubic phase. Thus, we conclude from the present data that the tetragonal $I4/mcm$ phase does not exist close to the cubic phase boundary. However, since the values of orthorhombic strain observed are near the limit of detectability for this technique, and peak broadening due to inhomogeneity could lead to systematic errors in refinement of the strain that would mask the intrinsic behavior, the question of whether the $I4/mcm$ phase exists between the *Ibmm* and $Pm\bar{3}m$ phases may require further investigation.

Measurements of the $(\frac{3}{2},\frac{1}{2},\frac{1}{2})_p$ superlattice peak intensity as a function of temperature for $x=0.3$ from the H4S spectrometer provide an explicit picture of the tempera-

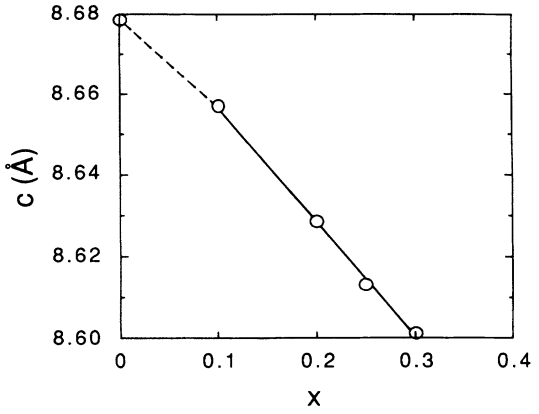

FIG. 9. The c-axis lattice parameter vs potassium concentration x in the orthorhombic *Ibmm* phase at 295 K. The point at $x=0$ in the monoclinic $I2/m$ phase is plotted for comparison.

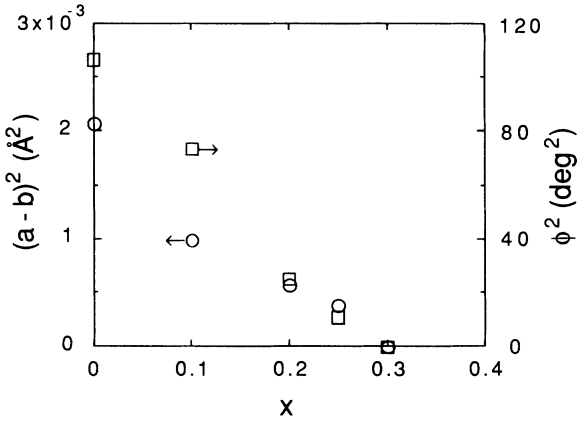

FIG. 10. The order parameters associated with the orthorhombic strain $(a-b)^2$ (circles) and the octahedral rotation angle ϕ^2 (squares) vs potassium concentration x in the orthorhombic *Ibmm* phase at 295 K. The points at $x=0$ in the monoclinic $I2/m$ phase are plotted for comparison.

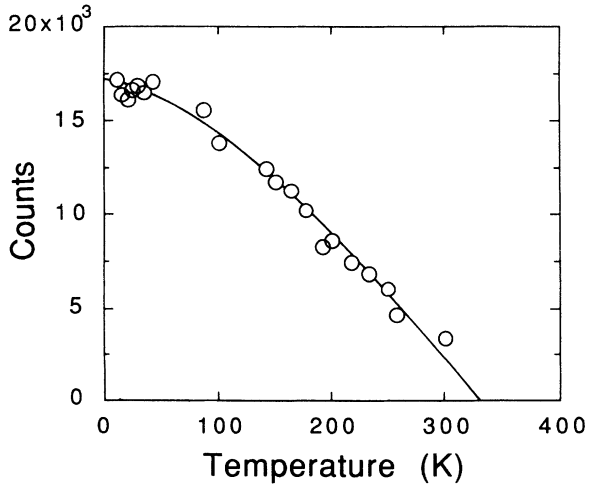

FIG. 11. Temperature dependence of the $(\frac{3}{2},\frac{1}{2},\frac{1}{2})$ superlattice peak intensity for $Ba_{0.7}K_{0.3}BiO_3$. The peak is indexed in terms of the primitive cubic cell.

ture dependence of the order parameter associated with the orthorhombic-cubic phase transition (Fig. 11). Again, the order-parameter behavior expected for a continuous transition is observed. The peak intensity extrapolates to zero at about 330 K, while the phase diagram inferred from Rietveld refinements of SEPD data (Fig. 3) suggests a transition temperature near 300 K.

D. Rhombohedral phase

The rhombohedral $R\bar{3}$ phase of $BaBiO_3$ was previously reported by Cox and Sleight.[16] In common with the monoclinic $I2/m$ phase, the rhombohedral $R\bar{3}$ phase contains combined octahedral tilt (in this case, along the $[111]_p$ direction) and breathing-mode distortions.

We observe a transition from the monoclinic to the rhombohedral phase at ~400 K for $x=0$, close to the temperature previously reported. We also observe the rhombohedral phase above room temperature for $x=0.1$. The Rietveld refinement profile for the $x=0$ data at 473 K is shown in Fig. 12, and the refined parameters are given in Table VII. The octahedral tilt angle is 9.1° and the difference in the Bi—O bond distances is 0.15 Å. These results agree well with those of Cox and Sleight.[16] For the $x=0.1$ sample above room temperature, refinements in the $R\bar{3}$ model also yielded satisfactory fits. Just as noted for the monoclinic phase, potassium substitution rapidly reduces the breathing-mode distortion in the rhombohedral phase. Compared with $BaBiO_3$, the $R\bar{3}$ structure at $x=0.1$ and 473 K is characterized by a smaller octahedral tilt (6.9°) and vanishingly small breathing-mode oxygen atom displacements. In the refinements for $x=0.1$, this decrease in the breathing-

TABLE VII. Refined structural parameters for $Ba_{1-x}K_xBiO_3$, $x=0$ and 0.1, at 473 K (200 °C). The data were refined in the rhombohedral $R\bar{3}$ space group. Numbers in parentheses are estimated standard deviations of the last significant digit. Where no standard deviation is given, the value was not refined.

		$x=0$	$x=0.1$
a (Å)		6.1520(1)	6.1423(1)
α (deg)		60.272(2)	60.143(4)
Ba	$x=y=z$	0.251(1)	0.251(2)
	B (Å^2)	1.44(4)	1.59(9)
	n	0.996(9)	0.93(3)
K	n	0	$1-n$(Ba)
Bi(1)	$x=y=z$	0	0
	B (Å^2)	0.75(8)	0.50(3)
	n	0.5	0.5
Bi(2)	$x=y=z$	$\frac{1}{2}$	$\frac{1}{2}$
	B (Å^2)	0.08(5)	$=B$[Bi(1)]
	n	0.5	0.5
O	x	−0.259(2)	−0.240(3)
	y	0.2126(6)	0.212(2)
	z	0.3040(6)	0.282(2)
	U_{11} (Å^2)	0.035(2)	0.040(3)
	U_{22} (Å^2)	0.024(2)	0.025(4)
	U_{33} (Å^2)	0.023(2)	0.034(5)
	U_{12} (Å^2)	−0.003(2)	−0.001(7)
	U_{13} (Å^2)	−0.005(3)	−0.013(8)
	U_{23} (Å^2)	−0.017(1)	−0.021(2)
	n	3	3
R_{wP} (%)		7.78	8.91
R_{exp} (%)		5.91	5.79

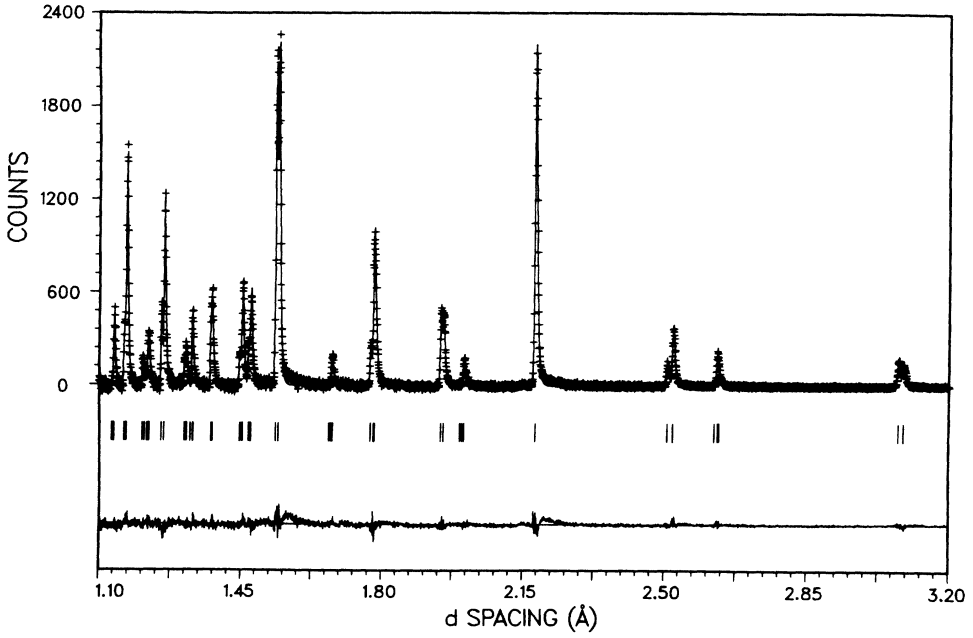

FIG. 12. A portion of the Rietveld refinement profile for rhombohedral ($R\bar{3}$) $BaBiO_3$ at 473 K (200 °C). The format is the same as Fig. 4.

mode distortions led to some convergence problems, since the two Bi sites became nearly equivalent. Additionally, for $x=0.1$, the rhombohedral distortions are small (rhombohedral angle $\alpha=60.14°$ at 473 K) making it difficult to establish the uniqueness of the $R\bar{3}$ structure directly from the raw data. We therefore attempted Rietveld refinements in several different space groups including *Ibmm*, *I4/mcm*, $R\bar{3}c$, and $R\bar{3}m$. In all cases, however, the $R\bar{3}$ structure was favored by *R*-value ratio tests.[41]

E. Primitive monoclinic phase

On cooling $BaBiO_3$ below 150 K, we consistently observed new Bragg peaks that could be indexed on the basis of a primitive monoclinic cell, with peak intensities that increased smoothly with cooling (Fig. 13). The variation of the refined monoclinic lattice parameters with temperature provides additional evidence for the transition from *I2/m* to a primitive monoclinic phase, as shown in Fig. 14. A rather pronounced anomaly is observed for the temperature dependence of the monoclinic angle β at about 140 K.

The Rietveld refinement of the $BaBiO_3$ data at 10 K was performed using the primitive monoclinic *P2/m* space group. This refinement converged and yielded a satisfactory fit. However, since the new primitive reflections are very weak, and the refinement is dominated by the strong primary reflections, *R*-value ratio tests[41] are of limited value and the identification of this structure may not be unique. Accordingly, the assignment of *P2/m* as the space group is only tentative. Moreover, since a primitive monoclinic phase was not reported in the earlier low-temperature study of $BaBiO_3$ by Thornton and Jacobsen,[27] its occurrence may depend critically on some sample-dependent variable (such as oxygen content) that we have not accurately characterized. Since the primitive monoclinic peaks were not observed in any data for $x=0.1$, the primitive monoclinic phase region does not extend to $x=0.1$.

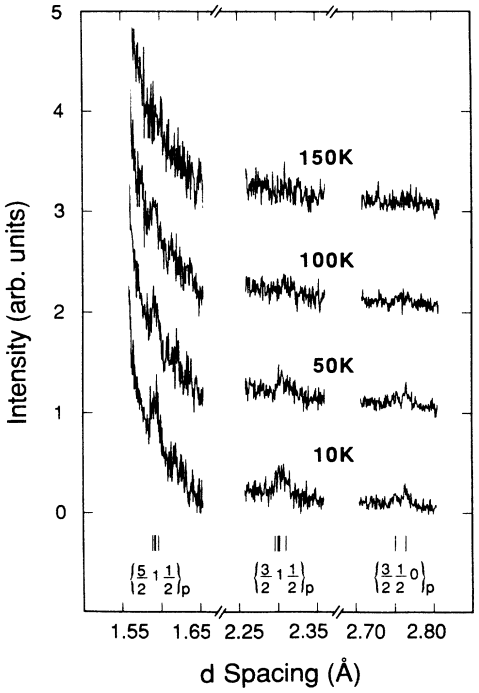

FIG. 13. Some of the primitive monoclinic Bragg peaks observed on cooling $BaBiO_3$. Tick marks below the profiles mark the positions of new peaks of the primitive monoclinic structure at 10 K. The Miller indices are given for a primitive pseudocubic unit cell. Note that these primitive peaks disappear at a temperature between 100 and 150 K.

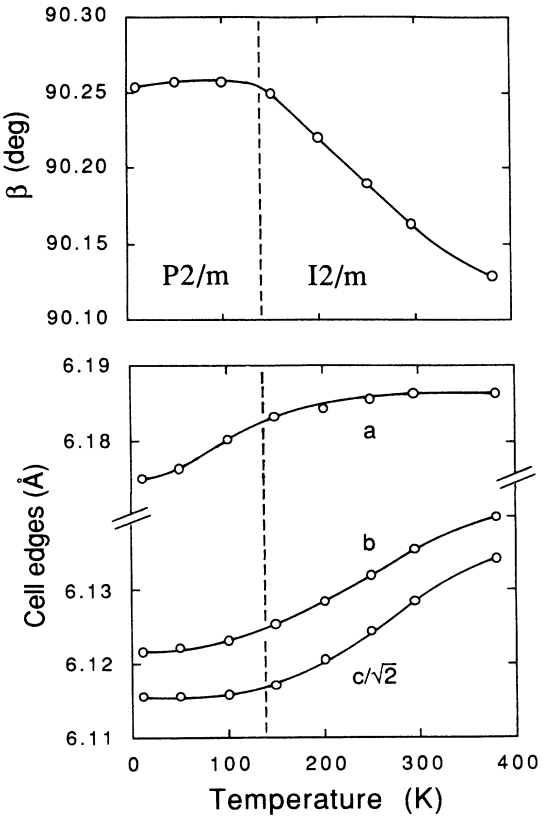

FIG. 14. Cell edges *a* and *b*, and *c* and monoclinic angle β for monoclinic $BaBiO_3$ vs temperature. The unusual change in slope for β near 140 K suggests a transition from body-centered (*I2/m*) to primitive monoclinic symmetry.

V. INCOMMENSURATE STRUCTURAL MODULATION

In addition to the commensurate structural modulations resulting from octahedral tilts and distortions, an incommensurate structural modulation has been observed in the $Ba_{1-x}K_xBiO_3$ system by electron diffraction.[26,32] Pei *et al.*[26] reported this modulation to have a wavelength that varied inversely with potassium concentration and suggested that it may be an incommensurate CDW. Hewat *et al.*[32] confirmed the existence of the modulation, but concluded that it was electron-beam induced and, thus, was not an intrinsic property of $Ba_{1-x}K_xBiO_3$. However, it should be noted that a similar modulation has also been observed by single-crystal x-ray diffraction

by Chaillout *et al.* in $BaBiO_{3-\delta}$.[42] They observed the wavelength of the modulation to be six times the primitive cubic (110) d spacing ($d_{(110)p}$), consistent with the subsequent electron-diffraction results. Furthermore, their work showed that the modulation wavelength did not change with the oxygen vacancy content (the same wavelength was observed for both $BaBiO_{2.97}$ and $BaBiO_{2.77}$), and concluded that it was highly unlikely that the modulation was the consequence of oxygen-vacancy ordering.

We have performed additional electron-diffraction studies of the incommensurate modulation as a function of x. The observed modulation wavelength as a function of x, along with the previous data of Pei *et al.*[26] and Hewat *et al.*,[32] is plotted in Fig. 15. The x-ray data of Chaillout *et al.*[42] for $x=0$ is not plotted but is in excellent agreement. The systematic variation of the modulation wavelength with potassium concentration indicates the same behavior for $BaBiO_3$ and potassium-substituted samples and, thus, argues against electron-beam-induced effects or oxygen-vacancy ordering as the explanation. These results suggest that the incommensurate structural modulation is an intrinsic property of the $Ba_{1-x}K_xBiO_3$ system. The report of Hewat *et al.*[32] that the modulation is induced by the electron beam could be explained if electron-beam heating increased the coherence length of an intrinsic short-range ordering or produced oxygen vacancies which then "dressed" an intrinsic modulation and, thus, increased the intensity of the superlattice spots.

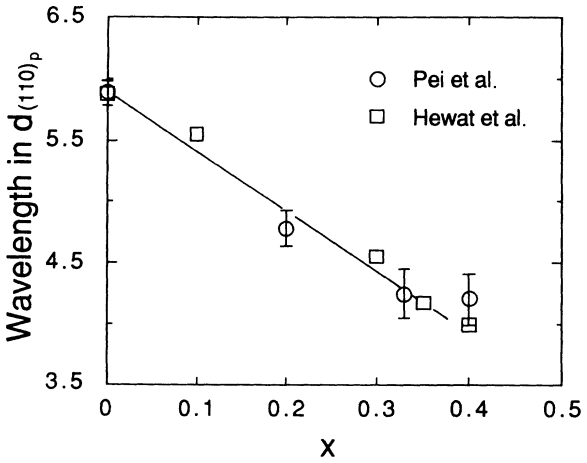

FIG. 15. The wavelength of the incommensurate modulation in $Ba_{1-x}K_xBiO_3$ vs x, as measured by electron diffraction. The wavelength is expressed in terms of the primitive cubic (110) d spacing, $d_{(110)p}$. The error bars show the range of wavelengths that are observed for different crystallites in a sample of nominal composition x. Circles are from Pei *et al.* (Ref. 26) and the present study and squares are the data of Hewat *et al.* (Ref. 32). In samples whose nominal compositions would be in the cubic phase ($x \geq 0.3$ at room temperature) some noncubic crystallites with an incommensurate modulation are observed (probably due to sample inhomogeneity). No modulation is observed in the cubic crystallites of the $x=0.4$ sample.

One purpose of the present work was to search for these incommensurate superlattice reflections using neutron diffraction. The H4S spectrometer offers the best sensitivity for weak reflections. In spite of careful searches at the wave vectors defined by the electron diffraction, none were observed. One possible explanation is that they are too weak to observe with neutron diffraction. Additionally, the peaks could be broadened by small domain size (which has been observed by electron-diffraction lattice imaging[26]). Our overall conclusion is that, without confirmation by an independent technique, or further investigation of electron-beam-induced processes, we cannot determine whether this modulation is an intrinsic property of bulk samples and, thus, potentially important to understanding the physics of the $Ba_{1-x}K_xBiO_3$ system.

VI. DISCUSSION

In summary, we have determined the structures which occur in the phase diagram of $Ba_{1-x}K_xBiO_3$ as a function of x and temperature (Fig. 3). Five distinct structures that can be understood in terms of simple tilting and breathing-mode distortions of the ideal cubic perovskite structure are observed. These structures are related by a logical progression of first tilting and then breathing-mode distortions upon decreasing x from the cubic phase.

The unit-cell distortions are rather small. In fact, the strains in the noncubic cells are so small that a pseudocubic lattice parameter can be assigned to all of the structures. At room temperature, this pseudocubic lattice parameter varies inversely with potassium content as shown in Fig. 16. The behavior is quite linear and provides a simple method for estimating x from the measured lattice parameter. Since the ionic radii of K^{1+} and Ba^{2+} are very similar (1.64 and 1.61 Å, respectively[43]), the observed decrease in unit-cell volume with x can be explained as a decrease in the size of the Bi ion as a result of its increased oxidation state. The ionic radii for Bi^{3+} and Bi^{5+} are, respectively, 1.03 and 0.76 Å.[43]

An important result of the present work is the identification of the semiconducting supercell phase adjacent to the cubic superconducting phase. Our data indicate an orthorhombic *Ibmm* structure, although a tetragonal *I4/mcm* structure cannot be completely ruled out. In either case, it is clear that this phase involves only tilting distortions. Although it is impossible to guarantee that our search for alternative structural models has been exhaustive, all of the models we have investigated involving breathing-mode distortions are strongly rejected on the basis of Rietveld refinements that are sensitive to the intensities of the supercell reflections. Thus, the argument that explains the loss of metallic behavior on the basis of a commensurate, long-range CDW (i.e., a breathing-mode distortion) which opens a gap in the density of states at the Fermi energy[18] is not consistent with the observations. Indeed, the rotational distortion, with a tilt angle that decreases to zero in a continuous way at the cubic phase transition, would not be expected to destroy metallic behavior.

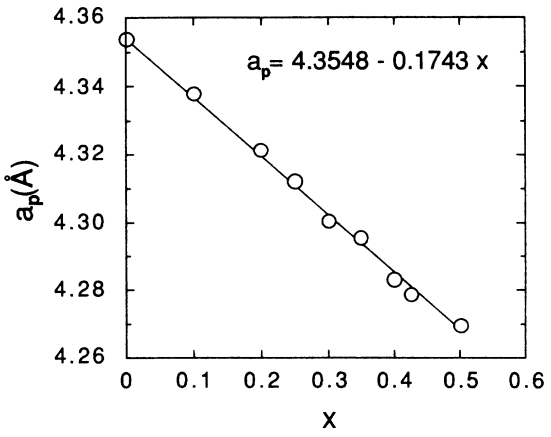

FIG. 16. Pseudocubic lattice parameter a_p vs potassium concentration x for the various phases of $Ba_{1-x}K_xBiO_3$. The straight line is a least-squares fit to the data and yields the equation $a_p = 4.3548 - 0.1743x$ which can be used to estimate x from measured lattice constants.

The puzzle of the normal-state resistivity in the $Ba_{1-x}K_xBiO_3$ system is likely to have the same origin as for the $BaPb_{1-x}Bi_xO_3$ system. With increasing Pb content in the latter system, the phases encountered at room temperature are[17]

$$I2/m \rightarrow O^{II} \rightarrow I4/mcm \rightarrow Ibmm .$$

Superconductivity occurs only in the $I4/mcm$ phase. The metal-insulator transition occurs at $x \approx 0.35$ (at the O^{II}-$I4/mcm$ transition), and semiconducting behavior is observed in the wide composition range up to $x=1$ ($BaBiO_3$). Although the structure of the O^{II} phase (existing over the range $0.35 < x < 0.95$) has not been reported, it is generally believed that the large Pb content should suppress the Bi charge disproportionation. The O^{II} structure is thus not expected to contain an ordered CDW that would produce a semiconducting gap.

Localization effects due to cation disorder alone are probably not sufficient to produce insulating behavior. Varma[21] has proposed that the correlation energy U on the Bi site can effectively become negative and has obtained a phase diagram indicating a CDW state that persists for finite hole concentrations, and borders a superconducting phase at lower temperature induced by the negative U correlations. In this model, the insulating state, even for finite substitution, is associated with an incommensurate CDW modulation achieved by rapid fluctuations of the valence on the Bi sites between +3 and +5. Similarly, Jurczek and Rice[19] have proposed for finite substitution a "local CDW" involving displacements of the oxygen atoms and charge fluctuations on the Bi sites, with an incommensurate periodicity. In their picture, a "pseudogap" (as has been observed in optical experiments[13,14,22]) still exists for finite substitution but the small number of states inside the gap are likely to be localized, thus keeping the material insulating.

The incommensurate modulation observed in $Ba_{1-x}K_xBiO_3$ by electron diffraction[26,32] could, of course, be the predicted CDW. However, the intrinsic nature of this incommensurate modulation has been challenged by the claim that it is electron-beam induced and, now, by the failure to observed it in the present neutron-diffraction study. The latter failure has three possible explanations: (a) The correlation length of the CDW state is very short (≤ 100 Å) and the corresponding peaks are too diffuse to see in the present powder samples. (b) The modulation fluctuates dynamically on a time scale too rapid to see in an elastic neutron-diffraction experiment. (c) The modulation is, in fact, an electron-beam-induced effect. The possible effects of beam heating include an increase of the coherence length of the modulation, thus creating long-range order where only short-range order is present intrinsically, or the creation of oxygen vacancies which order according to an underlying modulation.

From the commensurate structures determined in this study, we note that the absence of inequivalent Bi sites for $x \geq 0.1$ indicates that the Bi sites have equal valence (in a crystallographic average sense) throughout the system. However, locally they may adopt Bi^{3+} and Bi^{5+} configurations, with an instantaneous or even time-averaged short-range order. Such a local CDW model involving the disorder of Bi^{3+} and Bi^{5+} has been used by Chaillout *et al.*[28,29] to explain their data for the $BaBiO_3$ structure. Their neutron powder diffraction data revealed two types of $BaBiO_3$ structures for different samples at room temperature: One was characterized by a large difference in the two Bi—O bond lengths (~0.16 Å) and a large monoclinic angle while the other was characterized by almost equal Bi—O bond lengths and a smaller monoclinic angle. They proposed that the two structures were, respectively, 100 and 25 % ordered with respect to Bi^{3+} and Bi^{5+} cations.

The same local CDW model may be adopted to interpret the observed semiconducting behavior in the orthorhombic $Ibmm$ phase of $Ba_{1-x}K_xBiO_3$. Here, we assume that the degree of ordering of Bi^{3+} and Bi^{5+} on the two distinct Bi sites is continuously reduced by the substitution of potassium into $BaBiO_3$, and that it eventually becomes zero in the orthorhombic phase. The observed $Ibmm$ structure is, therefore, the disordered $I2/m$ structure with no long-range ordering of Ba^{3+} and Bi^{5+} cations on the lattice. Thus, the observed monoclinic-orthorhombic transition is in fact, an order-disorder transition involving the arrangement of Bi^{3+} and Bi^{5+} cations. In the context of this model, the orthorhombic phase contains the same breathing-mode distortion as $BaBiO_3$, but restricted to a local scale (i.e., a local CDW), leading, on average, to orthorhombic symmetry. The observed semiconducting behavior is a consequence of this local CDW.

It is tempting to draw an analogy between the CDW which competes with superconductivity in the $Ba_{1-x}K_xBiO_3$ system and antiferromagnetism in the copper-oxide superconductors. In the latter case, for both $La_{2-x}Sr_xCuO_4$ and $YBa_2Cu_3O_{7-x}$ the nonsuperconducting compositions exhibit antiferromagnetism.[44]

However, an important difference between the bismuthate and cuprate systems should be noted. In the case of $Ba_{1-x}K_xBiO_3$, the highest T_c is observed adjacent to the phase transition into the semiconducting phase, while in the cuprates, T_c drops steadily and superconductivity disappears before the antiferromagnetic phase is entered. This observation emphasizes again the importance of studying the metal-insulator transition in order to understand the mechanism of superconductivity in $Ba_{1-x}K_xBiO_3$.

ACKNOWLEDGMENTS

The work at Argonne National Laboratory was supported by the U.S. Department of Energy, Division of Basic Energy Sciences—Materials Sciences, under Contract No. W-31-109-ENG-38 (J.D.J., D.G.H., and A.W.M.), the National Science Foundation Science and Technology Center for Superconductivity under Grant No. DMR-88-09854 (S.P. and B.D.), and American Air Liquide, Inc. (D.R.).

[1]L. F. Mattheiss, E. M. Gyorgy, and D. W. Johnson, Jr., Phys. Rev. B **37**, 3745 (1988).

[2]R. J. Cava, B. Batlogg, J. J. Krajewski, R. C. Farrow, L. W. Rupp, Jr., A. E. White, K. T. Short, W. F. Peck, Jr., and T. Y. Kometani, Nature **332**, 814 (1988).

[3]D. G. Hinks, B. Dabrowski, J. D. Jorgensen, A. W. Mitchell, D. R. Richards, Shiyou Pei, and Donglu Shi, Nature **333**, 836 (1988).

[4]S. Kondoh, M. Sera, Y. Ando, and M. Sato, Physica C **157**, 469 (1989).

[5]Y. Uemura, B. J. Sternlieb, D. E. Cox, J. H. Brewer, R. Kadono, J. R. Kempton, R. F. Kiefl, S. R. Kreitzman, G. M. Luke, P. Mulhern, T. Riseman, D. L. Williams, W. J. Kossler, X. H. Yu, C. E. Stronach, M. A. Subramanian, J. Gopalakrishnan, and A. W. Sleight, Nature **335**, 151 (1988).

[6]D. G. Hinks, D. R. Richards, B. Dabrowski, D. T. Marx, and A. W. Mitchell, Nature **335**, 419 (1988).

[7]B. Batlogg, R. J. Cava, L. W. Rupp, Jr., A. M. Mujsce, J. J. Krajewski, J. P. Remieka, W. F. Peck, Jr., A. S. Cooper, and G. P. Espinosa, Phys. Rev. Lett. **61**, 1670 (1988).

[8]Z. Schlesinger, R. T. Collins, J. A. Calise, D. G. Hinks, A. W. Mitchell, Y. Zheng, B. Dabrowski, N. E. Bickers, and D. J. Scalapino, Phys. Rev. B **40**, 6862 (1989).

[9]C.-K. Loong, P. Vashishta, R. K. Kalia, M. H. Degani, D. L. Price, J. D. Jorgensen, D. G. Hinks, B. Dabrowski, A. W. Mitchell, D. R. Richards, and Y. Zheng, Phys. Rev. Lett. **62**, 2628 (1989).

[10]J. F. Zasadzinski, N. Tralshawala, D. G. Hinks, B. Dabrowski, A. W. Mitchell, and D. R. Richards, Physica C **158**, 519 (1989).

[11]D. G. Hinks, B. Dabrowski, D. R. Richards, J. D. Jorgensen, Shiyou Pei, J. F. Zasadzinski, in *High-Temperature Superconductors: Relationship between Properties, Structure, and Solid State Chemistry, San Diego, 1989,* Proceedings of the Materials Research Society, edited by J. D. Jorgensen, K. Kitazaur, J. M. Tarascon, M. S. Thompson, and J. B. Torrance (Materials Research Society, Pittsburgh, Kansas, 1989), Vol. 156, pp. 357–367.

[12]B. Dabrowski, D. G. Hinks, J. D. Jorgensen, R. K. Kalia, P. Vashishta, D. R. Richards, D. T. Marx, and A. W. Mitchell, Physica C **156**, 24 (1988).

[13]H. Sato, S. Tajima, H. Takagi, and S. Uchida, Nature **338**, 241 (1989).

[14]For a review of the work on $BaPb_{1-x}Bi_xO_3$ see, S. Uchida, K. Kitazawa, and S. Tanaka, Phase Transitions **8**, 95 (1987).

[15]D. E. Cox and A. W. Sleight, Solid State Commun. **19**, 969 (1976).

[16]D. E. Cox and A. W. Sleight, Acta Crystallogr. B **35**, 1 (1979).

[17]D. E. Cox and A. W. Sleight, in *Proceedings of the Conference on Neutron Scattering, Gatlinburg, 1976,* edited by R. M. Moon (National Technical Information Service, Springfield, Virginia, 1976), pp. 45–54.

[18]L. F. Mattheiss and D. R. Hamann, Phys. Rev. B **28**, 4227 (1983).

[19]E. Jurczek and T. M. Rice, Europhys. Lett. **1**, 255 (1986).

[20]W. Weber, Jpn. J. Appl. Phys. **26**, Suppl. 3, 981 (1987).

[21]C. M. Varma, Phys. Rev. Lett. **61**, 2713 (1988).

[22]S. Tajima, S. Uchida, K. Kitazawa, S. Tanaka, and N. Terame, Phys. Rev. B **32**, 6302 (1985); S. Tajima, S. Uchida, A. Masaki, H. Takagi, K. Kitzawa, and S. Tanaka, *ibid.* **35**, 696 (1987).

[23]R. M. Fleming, P. Marsh, R. J. Cava, and J. J. Krajewski, Phys. Rev. B **38**, 7076 (1988).

[24]G. H. Kwei, J. A. Goldstone, A. C. Lawson, Jr., J. D. Thompson, and A. Williams, Phys. Rev. B **39**, 7378 (1989).

[25]M. T. Weller, J. R. Grasmeder, P. C. Lanchester, P. A. J. DeGroot, G. P. Rapson, and A. C. Hannon, Physica C **156**, 265 (1988).

[26]Shiyou Pei, N. J. Zaluzec, J. D. Jorgensen, B. Dabrowski, D. G. Hinks, A. W. Mitchell, and D. R. Richards, Phys. Rev. B **39**, 811 (1989).

[27]G. Thornton and A. J. Jacobsen, Acta Crystallogr. B **34**, 351 (1978).

[28]C. Chaillout, J. P. Remeika, A. Santoro, and M. Marezio, Solid State Commun. **56**, 833 (1985).

[29]C. Chaillout, A. Santoro, J. P. Remeika, A. S. Cooper, G. P Espinosa, and M. Marezio, Solid State Commun. **65**, 1363 (1988).

[30]J. P. Wignacourt, J. S. Swinnea, H. Steinfink, and J. B. Goodenough, Appl. Phys. Lett. **53**, 1753 (1988).

[31]L. F. Schneemeyer, J. K. Thomas, T. Seigrist, B. Batlogg, L. W. Rupp, R. L. Opila, R. J. Cava, and D. W. Murphy, Nature **335**, 421 (1988).

[32]E. A. Hewat, C. Chaillout, M. Godinho, M. F. Gorius, and M. Marezio, Physica C **157**, 228 (1989).

[33]D. G. Hinks, D. R. Richards, B. Dabrowski, A. W. Mitchell, J. D. Jorgensen, and D. T. Marx, Physica C **156**, 477 (1988).

[34]U. Welp, W. K. Kwok, G. W. Crabtree, H. Claus, K. G. Vandervoort, B. Dabrowski, A. W. Mithcell, D. R. Richards, D. T. Marx, and D. G. Hinks, Physica C **156**, 27 (1988).

[35]J. D. Jorgensen, J. Faber, Jr., J. M. Carpenter, R. K. Crawford, J. R. Haumann, R. L. Hitterman, R. Kleb, G. E. Ostrowski, F. J. Rotella, and T. G. Worlton, J. Appl. Crystallogr. **22**, 321 (1989).

[36]R. B. VonDreele, J. D. Jorgensen, and C. G. Windsor, J. Appl. Crystallogr. **15**, 581 (1982).

[37]A. M. Glazer, Acta Crystallogr. A **28**, 3384 (1972).

[38]A. M. Glazer, Acta Crystallogr. A **31**, 756 (1975).

[39]V. F. Sears, in *Methods of Experimental Physics,* Vol. 23 of *Neutron Scattering,* edited by K. Sköld and D. L. Price (Academic, Orlando, 1987), Part A, p. 541.

[40]B. Dabrowski, D. G. Hinks, J. D. Jorgensen, D. R. Richards, Shiyou Pei, Y. Zheng, and A. W. Mitchell, J. Non-Crystall. Solids (to be published).

[41]*International Tables for X-Ray Crystallography* (Kynoch, Birmingham, 1974), Vol. IV, p. 288; W. C. Hamilton, Acta Crystallogr. **18**, 502 (1965).

[42]C. Chaillout and J. P. Remeika, Solid State Commun. **56**, 833 (1985).

[43]R. D. Shannon, Acta Crystallogr. A **32**, 751 (1976).

[44]See, for example, S. K. Sinha, Mater. Res. Bull. **13**, 24 (1988), and the references cited therein.